Wave propagation in rods with an exponentially varying cross-section – modelling and experiments

Michał K Kalkowski, Jen M Muggleton and Emiliano Rustighi
University of Southampton, Highfield, Southampton SO17 1BJ, UK
E-mail: M.Kalkowski@soton.ac.uk

Abstract. In this paper we analyse longitudinal wave propagation in exponentially tapered rods from both a theoretical and an experimental perspective. The tapering introduces significant changes to the behaviour of the rod. The longitudinal wave does not propagate from zero frequency, its cut-off frequency depending on the coefficient in the exponent. The analytical description of this phenomenon is well established, however little experimental work has been published to date. After a brief review of the classical solution of the exponential rod equation, we derive a methodology allowing the wavenumbers to be estimated from a set of equally spaced dynamic responses. Our approach is verified numerically against a finite element simulation and validated experimentally, both showing very good agreement. To further explain the results and provide an outlook for future work, we present a finite element model of the tapered rod embedded in an infinite solid medium. We conclude with a discussion on the effects of the surrounding medium on the behaviour of the structure and resulting characteristic features of the wavenumber.

1. Introduction

Waves in tapered rods have been widely studied throughout the years and many classical solutions are available in the literature with the acoustic horn as the foremost example [1]. One of the most typical features of such structures is banded energy transmission related to the cut-off reqion. To study the phenomena resulting from the tapering, a variety of mathematical treatments has been applied. Stevenson [2] used the WKB approximation to formulate solutions for horns of an arbitrary shape enabling the identification of transmission and attenuation zones. Nayfeh and Telionis [3] employed the multiple scales method to study wave propagation in ducts with a varying cross-section. For specific tapering configurations, longitudinal wave propagation and vibration were described using Bessel functions [4, 5]. Finally, Langley [6] performed an extensive investigation into wave propagation in non-homogeneous waveguides (including both longitudnal and flexural motion) with the aid of perturbation methods.

Exponential tapering, which is of interest in this paper, allows for an analytical solution, if the elementary rod theory is used. However, more complex rod theories may well be addressed by the aforementioned methods. One other possible approach is to formulate the problem in a transfer matrix manner [7]. Based on that concept, Gan et al. [8] presented a study comparing different rod theories for non-uniform rods focusing on pass-bands and cut-off frequencies.

Whilst wave propagation in tapered bars placed in an industrial context is the most common research motivation, certain types of tapering are observed in naturally grown structures. For instance, it is known that tree roots' diameter decreases exponentially in the vicinity of the

stem, which is commonly referred to as the 'zone of rapid taper' [9]. In recent years there has been an increased interest in exploration and maintenance of the underground space, especially in an urban environment. In this light, non-destructive methods capable of interrogating buried components using on-surface measurements are of primary interest. Building on the successful application of vibroacoustic methods for locating buried water pipes [10], similar principles are expected to support remote tree root detection. To envisage the latter, a better understanding of wave propagation in root structures and how they radiate into the surrounding soil is required.

The most simplistic representation of a tree root is an exponentially tapered rod. Given the background application, the primary focus of the work presented in this paper was put on an experimental investigation of waves in such structures. Although the literature on the topic is extensive, to our best knowledge, experimental results on wavenumbers in exponentially tapered solid rods were published.

In this paper we propose a methodology enabling wavenumbers in exponentially tapered rods to be estimated from a set of equally spaced measurements. The experimental results are compared with established theoretical solutions and various features of the gathered data discussed. Motivated by the background application, we also discuss the expected influence of the surrounding soil based on preliminary finite element simulations.

The paper is organised as follows. In Section 2, we briefly present the analytical model for an exponentially tapered rod. In Section 3, the equations for the estimation of the wavenumbers from five measured dynamic responses are derived and verified with a numerical experiment. The experiments including both frequency response function (FRF) measurement and wavenumber estimation are presented in Section 4. Finally, the results from preliminary finite element simulations are presented to support the discussion on the effect of surrounding soil on wave propagation in Section 5.

2. Analytical model

Longitudinal wave propagation is analysed using the elementary rod theory that assumes a uniform distribution of the displacement and neglects the effects of Poisson's contraction. The displacement is taken time-harmonic and the $\mathrm{e}^{\jmath\omega t}$ term is omitted hereafter for clarity. The equation of motion in the frequency domain is [11]

$$U''(x) + \frac{A'(x)}{A(x)}U'(x) + \omega^2\frac{\rho}{E}U(x) = 0 \tag{1}$$

where $U(x)$ is the complex amplitude of the displacement, $A(x)$ is the cross-sectional area of the rod, ρ is the density, E is the Young's modulus and the prime denotes differentiation over the propagation direction, x. Noting that the exponential tapering yields an x-dependence of the radius r

$$r(x) = r_0\mathrm{e}^{-\beta x} \tag{2}$$

the governing equation can be written in a simpler form

$$U''(x) - 2\beta U'(x) + \omega^2\frac{\rho}{E}U(x) = 0 \tag{3}$$

The form of tapering considered in this paper results in equation (3) having constant coefficients. Owing to that, an analytical solution is available. Assuming that $U(x) = U\mathrm{e}^{-\jmath kx}$, where U is the complex wave amplitude and k is the wavenumber, we obtain

$$-k^2 + \jmath 2\beta k + \omega^2\frac{\rho}{E} = 0 \tag{4}$$

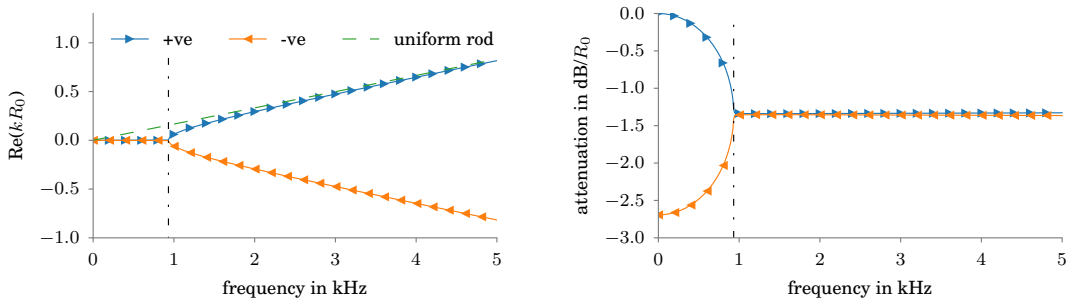

Figure 1. Dispersion curves for an exponentially tapered rod.

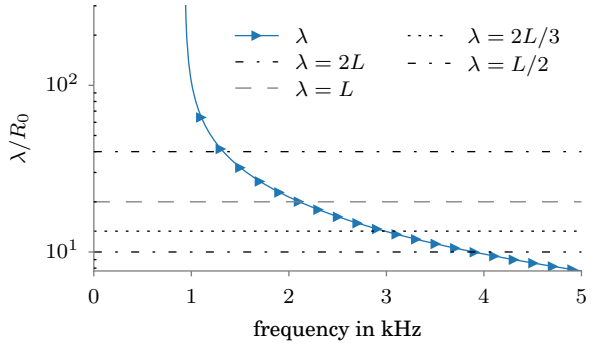

Figure 2. Longitudinal wavelength in the exponentially tapered rod against frequency; lines corresponding to certain number of wavelengths within the length of the rod are also marked.

from which the wavenumbers are calculated as

$$k = \frac{-\jmath 2\beta \pm \sqrt{-4\beta^2 + 4k_n^2}}{-2} = \jmath\beta \mp \sqrt{-\beta^2 + k_n^2} \tag{5}$$

In the above equation, k_n^2 denotes the square of the uniform rod wavenumber $\left(\omega^2 \frac{\rho}{E}\right)$.

A brief inspection of equation (5) indicates that there exists a cut-off frequency ($\omega = \beta c_L$) below which both wavenumbers are imaginary, i.e. the associated waves are evanescent. Above the cut-off frequency there are two propagating waves – negative- and positive going. The amplitude of the positive-going wave (in the direction of diminishing radius) grows, whereas the amplitude of the negative-going wave decreases, as indicated by the imaginary part of the wavenumber. At high frequencies the real part of the wavenumber of the tapered rod approaches the uniform rod solution.

In Figure 1 we plot illustrative dispersion curves for a circular exponentially tapered rod ($E = 10 \times (1 + 0.005j)$ GPa, $\rho = 700$ kg/m^3, $\beta = 1.55$, $R_0 = 0.1$ m). The cut-off phenomenon is clearly visible, although since the material is damped the real part of the wavenumber is non-zero in the cut-off region. It is known that no purely imaginary wavenumbers can exist in lossy structures and that the real part of the wavenumber is always non-zero (albeit often very small). The analytical cut-off frequency (932 Hz) is marked in Figure 1 for reference. The longitudinal wavelength as a function of frequency is plotted in Figure 2. For a free-free tapered rod, the frequencies at which there is an integer number of half-wavelengths along the rod correspond to its natural frequencies.

3. Estimating wavenumbers from equidistant FRFs

In this paper we aimed at establishing a sensor configuration for measuring the wavenumbers in exponentially tapered rods. One possible approach was presented by Muggleton et al. [12] who estimated wavenumbers in a pipe using dynamic responses taken at three equispaced locations. Their method originated from the observation that the steady-state response is a superposition of waves travelling across the structure. As only one wave type was expected to be propagating in that case and $k^+ = -k^-$, simple relationships was derived.

3.1. Derivation

For an exponentially tapered rod the positive- and negative-going wavenumbers are different, i.e. $k^+ \neq -k^-$. Consequently, we assumed the response to be a function of two unrelated wavenumbers

$$u(x,t) = u_1 \mathrm{e}^{\jmath(\omega t - k_1 x)} + u_2 \mathrm{e}^{\jmath(\omega t - k_2 x)} \tag{6}$$

where k_1 and k_2 are the two wavenumbers and u_1 and u_2 are the associated wave amplitudes. Note that no attribution of the direction of propagation is made at this stage.

The number of required sensing location comes from the number of unknowns (wavenumbers and wave amplitudes) and the form of equation (6). Muggleton et al. [12] showed that three sensing locations suffice if there is only one wave type propagating and $k^+ = -k^-$. In the case presented here there are four unknowns in total (see equation (6)). However, we found that convenient manipulation of a set of sums of exponential terms can be done if five sensing locations are used (resulting in five simultaneous equations).

Dropping the time-harmonic term and denoting the spacing between the sensors as L_s five equispaced displacements $u_{a\ldots e}$ can be written as

$$\begin{aligned}
u_a &= u_1 \mathrm{e}^{-\jmath k_1 x_0} + u_2 \mathrm{e}^{-\jmath k_2 x_0} \\
u_b &= u_1 \mathrm{e}^{-\jmath k_1 (x_0 + L_s)} + u_2 \mathrm{e}^{-\jmath k_2 (x_0 + L_s)} \\
u_c &= u_1 \mathrm{e}^{-\jmath k_1 (x_0 + 2L_s)} + u_2 \mathrm{e}^{-\jmath k_2 (x_0 + 2L_s)} \\
u_d &= u_1 \mathrm{e}^{-\jmath k_1 (x_0 - L_s)} + u_2 \mathrm{e}^{-\jmath k_2 (x_0 - L_s)} \\
u_e &= u_1 \mathrm{e}^{-\jmath k_1 (x_0 - 2L_s)} + u_2 \mathrm{e}^{-\jmath k_2 (x_0 - 2L_s)}
\end{aligned} \tag{7}$$

where x_0 is the location of the central sensor with respect to a chosen origin.

A series of arithmetic manipulations of the above equations leads to the following set of simultaneous equations

$$\begin{aligned}
\mathrm{e}^{\jmath k_1 L} + \mathrm{e}^{\jmath k_2 L} &= C_1 \\
\mathrm{e}^{-\jmath k_1 L} + \mathrm{e}^{-\jmath k_2 L} &= C_2
\end{aligned} \tag{8}$$

where $C_1 = \dfrac{u_b u_e - u_a u_d}{u_b u_d - u_a^2}$ and $C_2 = \dfrac{u_d u_c - u_a u_b}{u_b u_d - u_a^2}$.

Equation (8) can be solved by substitution

$$\mathrm{e}^{\jmath k_2 L} = \frac{1}{C_2 - \mathrm{e}^{-\jmath k_1 L}} \tag{9}$$

which leads to

$$C_2 \mathrm{e}^{2\jmath k_1 L} - C_1 C_2 \mathrm{e}^{\jmath k_1 L} + C_1 = 0 \tag{10}$$

Equation (10) is an ordinary quadratic equation, so

$$\mathrm{e}^{\jmath k_1 L} = \frac{C_1 C_2 \pm \sqrt{C_1 C_2 (C_1 C_2 - 4)}}{2C_2} \tag{11}$$

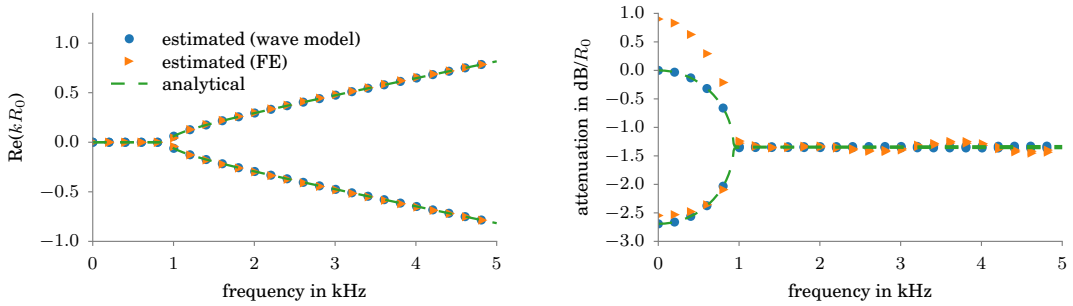

Figure 3. Numerical verification of the wavenumber estimation procedure based on an analytical forced response model and a finite element model.

Finally, the wavenumber is obtained from

$$k_1 = \frac{1}{\jmath L} \ln \left(\frac{C_1 C_2 \pm \sqrt{C_1 C_2 (C_1 C_2 - 4)}}{2 C_2} \right) \tag{12}$$

The right hand side of equation (11) is a complex number, so a complex definition of logarithm must be used while evaluating k_1 in equation (12). The other wavenumber is obtained from the substitution equation, yet the analysis of the form of equation (8) indicates that the pairs of solutions for k_1 and k_2 are identical. Hence it is enough to solve the above equation for k_1 which then captures both wavenumbers.

3.2. Numerical example for an analytical and an FE model

The methodology is verified numerically using a wave-based forced response model (see Appendix) and a finite element model. The cross-sectional dimensions and properties of the rod are the same as in the preceding section except for the length which is specified now to be 2 m. The sensors are spaced at 0.3 m starting from the location 0.15 m from the large face. Corresponding wavenumber estimates are shown in Figure 3.

The results confirm that the wavenumbers are estimated correctly using the proposed routine. The results from the FE model are not very accurate in the cut-off region which is related to the mesh density. As the phase variation of the response along the rod is very small in that region, one needs a very fine mesh to represent these effects correctly (much finer than the typical convergence criteria). We conducted a short study, results of which are not shown here, that confirmed that hypothesis.

4. Experiments

We performed a series of experiments on a freely suspended wooden rod with an exponentially varying radius. The rod was 2.006 m long and its radius varied from 0.945 to 0.004 m in an exponential manner. The density and an effective Young's modulus in the axial direction were estimated based on the measured FRFs.

The experimental setup is schematically depicted in Figure 4(a) and shown on a photograph in Figure 5. The rod was excited with an electrodynamic shaker at the end with larger radius and instrumented with PCB 35C22 accelerometers. The input force was measured by a PCB208C01 force gauge connected to a shaker via a stinger. At each sensing location we used four accelerometers evenly distributed around the circumference as shown in Figure 4(b). This enabled the influence of flexural waves, which were excited due to a non-ideally axial forcing and material anisotropy, to be cancelled. The accelerometers were mounted on the surface of the rod

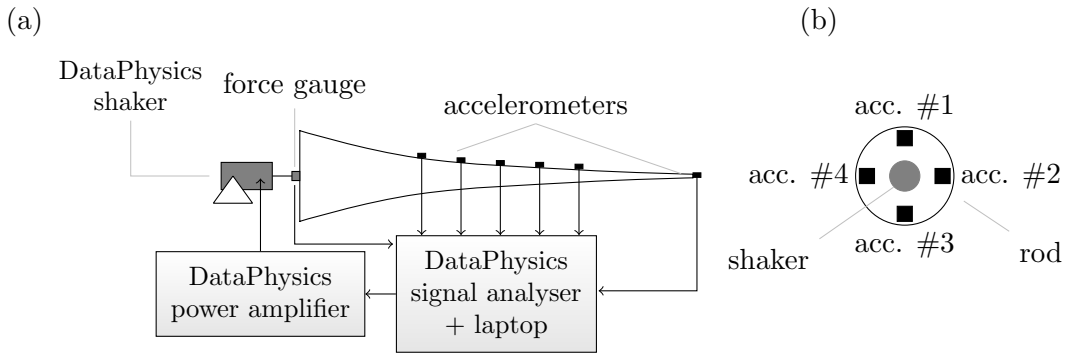

Figure 4. Experimental setup for longitudinal FRF measurement: (a) schematic diagram; (b) accelerometers arrangement for longitudinal input FRF measurement (planar view of the large face)

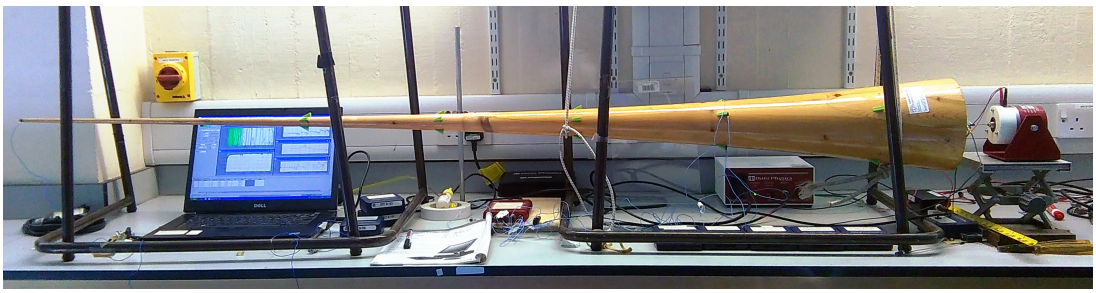

Figure 5. A photograph of the experimental setup

using 3D-printed attachments to facilitate orienting them so that predominantly longitudinal response was captured.

The results for the point and transfer FRFs are shown in Figure 6, where the predicted results are computed using the updated properties ($E = 13.89 \times (1 + 0.0073j)$ GPa, $\rho = 531$ kg/m^3, $\beta = 1.643$, $L = 2.007$). There are three resonances visible which correspond to when an integer number of a half-wavelength matches the length of the rod. Imprints of flexural resonances, the presence of which was alluded to above, can be observed in the transfer FRF (Figure 6) below 2 kHz.

4.1. Wavenumber estimation

In this section we apply the method described in Sec. 3 to a set of responses measured experimentally at five equally spaced locations. The sensors' spacing has a significant effect on the quality and, possibly, required processing of the estimates [12]. Whilst a too small spacing (compared with the wavelength) makes the inversion procedure very prone noise, largely spaced sensors (more than half a wavelength apart) suffer from spatial aliasing, providing a wrapped estimate of the wavenumber. The method discussed in this paper requires some *a priori* knowledge of the expected wavelengths, so that the sensors' spacing can be chosen accordingly. For this experiment, the sensors were spaced at 0.3 m (starting sensor at 0.15 m from the shaker) which ensured that no spatial aliasing would occur.

Wavenumber estimates from the experimental data are compared with the analytical result in Figure 7. The estimates follow the analytical trend closely and the cut-off phenomenon is well predicted. The resonance imprints on the estimates (e.g around 4.5 kHz) are thought to be related to residual flexural motion contribution.

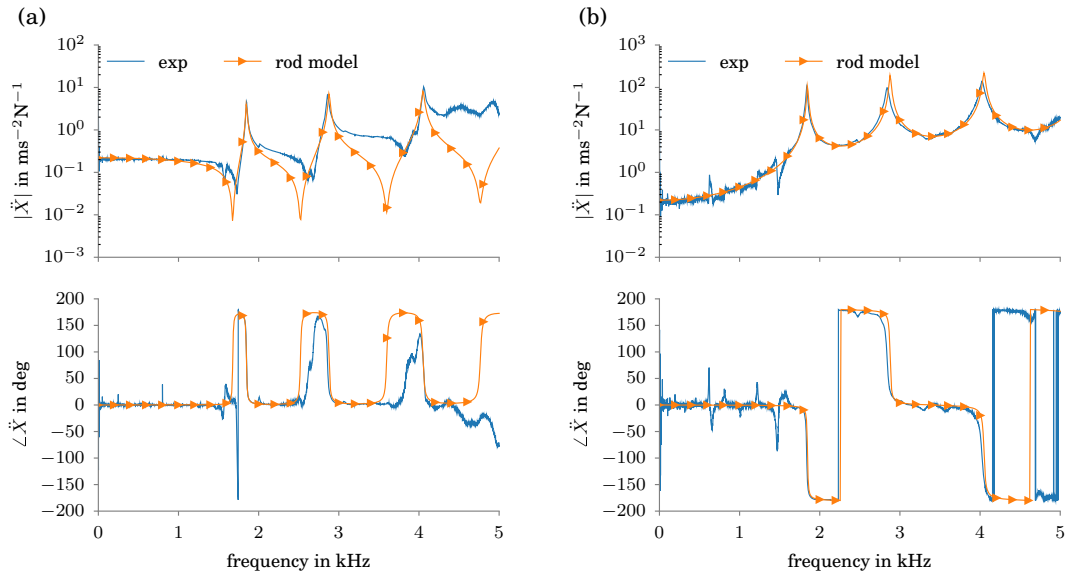

Figure 6. Point(a) and transfer(b) accelerances for an exponentially tapered rod – comparison between the experimental results and the analytical results based on rod's updated properties.

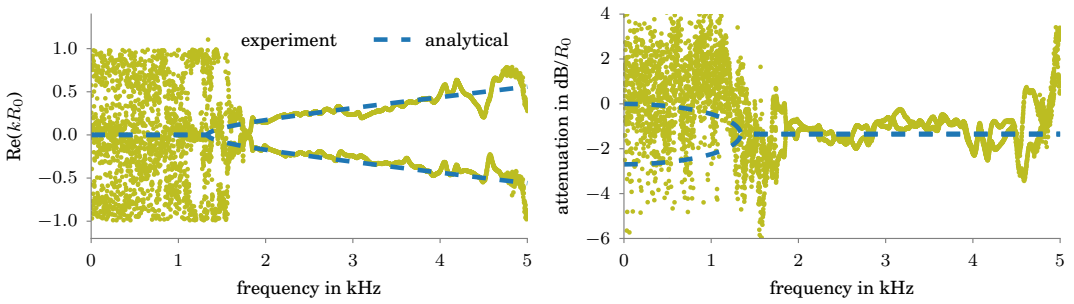

Figure 7. Longitudinal wavenumber estimated from the experimental data (using the ring of four sensors at each location).

The results below the cut-off frequency deserve a further explanation. In this region the wavenumber is predominantly imaginary, hence the phase difference between the responses along the rod is very small. Consequently, the outcome of the arithmetic manipulation of the dynamic responses used to estimate wavenumbers is dominated by measurement noise and contains little useful physical information. Owing to the numerical implementation of the logarithm, the wavenumber is limited to $(-\pi L_s, \pi L_s)$ range (with L_s being the sensors' spacing) which explains the arrangement of points in Figure 7 and also suggests that the wave is, indeed, cut off.

The results in the propagating region are promising and prove the potential of the method for measuring wavenumbers in exponentially tapered rods. However, predominantly imaginary wavenumbers cannot be recovered if signals are noisy.

The significance of an appropriate choice for sensors' spacing is demonstrated in Figure 8 where the results with 0.15 m spacing are shown. The estimates are strongly affected by noise and extracting physical information becomes difficult.

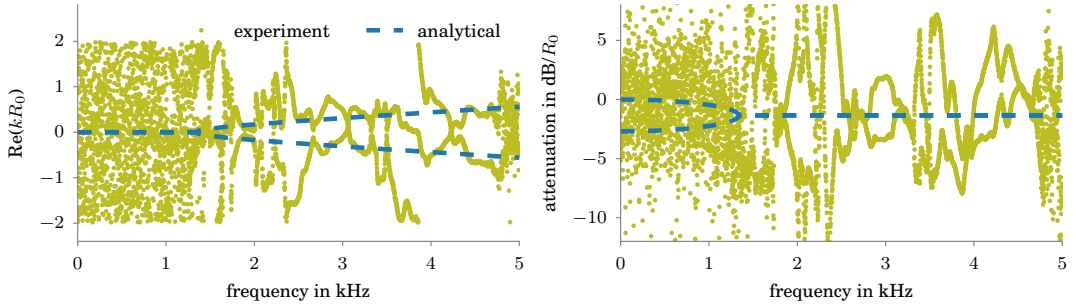

Figure 8. Longitudinal wavenumber estimated from the experimental data - the effect of insufficient sensor spacing (here: 0.15 m).

5. The effect of the surrounding medium on waves in an embedded rod

In this section we look at the influence of the surrounding medium on longitudinal waves in exponentially tapered rods with the aid of finite element simulations. Preliminary results presented below are expected to inform future experimental work.

Two configurations were considered: (i) exponential rod embedded in a finite cuboid of sand with free boundaries (3D FE model); (ii) exponential rod embedded in an infinite soil (axisymmetric 2D FE model). The former relates directly to a planned experiment in which the wooden rod will be placed in a large sandbox with sensors installed so that an analogous measurement campaign can be performed. The latter configuration provides insight into the effect of the infinite soil on guided wave propagation along the rod.

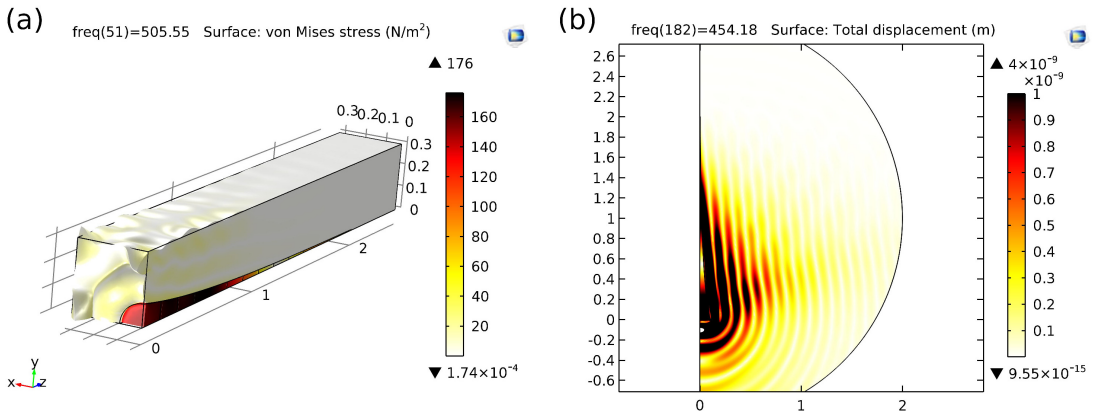

Figure 9. Illustrative results from the FE models: (a) at 505 Hz for the rod embedded in a finite block of sand; (b) at 454 Hz for the rod embedded in a soil with low-reflective boundaries (axisymmetric model)

5.1. Rod embedded in a finite sandbox (3D model)

In this model, an exponentially tapered rod with dimensions and properties as in Section 4 was placed in a finite cuboid of sand ($0.6 \times 0.6 \times 2.5$ m) emulating a sandbox planned for future laboratory experiments. The force was applied to the large face of the rod which was aligned with one of the small walls of the sandbox. The walls of the box were not modelled and the sand surfaces were assumed to be free. Sand was represented as an isotropic material with $c_L = 161.446 + \jmath 8.0522$ m/s, $c_S = 100.1246 + \jmath 4.9938$ m/s, $\rho = 2000$ kg/m^3, where the loss

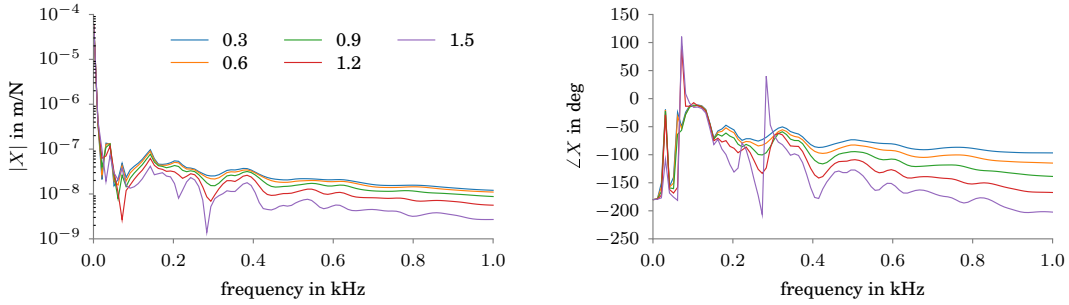

Figure 10. Transfer functions measured at locations specified in the legend to be used for wavenumber estimation.

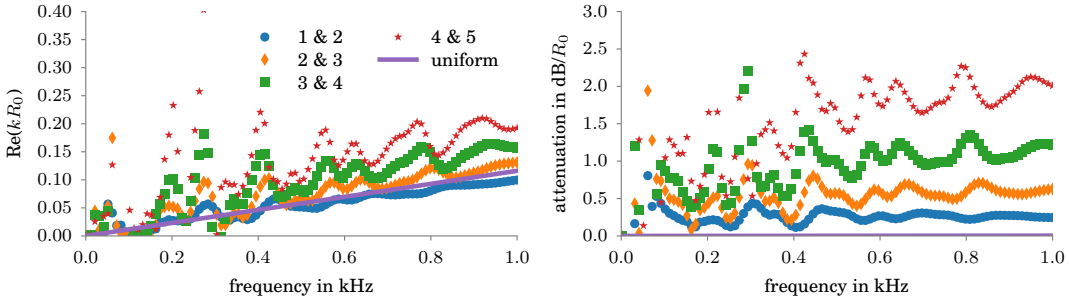

Figure 11. Wavenumbers for an exponential rod in a finite sandbox calculated from different pairs of adjacent sensing locations.

factor η was 0.1. Finally, the surface of the rod was considered to be in compact contact with the sand, allowing no relative displacement between the rod and the sand. For convenience, we modelled only a quarter of the described configuration and prescribed symmetry boundary conditions on two faces. The model consisted of 247816 quadratic tetrahedral elements (with the minimum element size equal to a quarter of the shortest wavelength, as recommended for quadratic elements). An illustrative example of the results as visualised by the FE package is shown in Figure 9(a).

The response was measured at five locations spaced at 0.3 m starting from the location 0.15 m from the force. The corresponding FRFs are shown in Figure 10. Here, the waves can be seen to decay towards the thinner end of the rod. Moreover, the resonances are very weak and hardly visible at locations far from the tip. This indicates that a very small reflected wave is present and owing to attenuation it contributes mainly to the response close to the tip. The above-mentioned observations suggest that the five sensors approach described in Section 3 is not appropriate and a simpler methodology can be adopted in which the space harmonic component is extracted from two adjacent responses

$$\mathrm{e}^{-\jmath kL} = \frac{u_b}{u_a} \tag{13}$$

We calculated the estimate using equation (13) for all pairs of adjacent sensing locations as described above. The results are presented in Figure 11 with a few features immediately apparent. Firstly, the cut-off phenomenon does not exist any more and waves propagate from zero frequency. Secondly, the trend lines for all locations are different indicating that the wavenumber varies along the rod. In this case the calculation from equation (13) gives only

an approximate wavenumber over the sensors' spacing L_s. In addition to that, the wave does not grow while propagating down the rod, but decays with attenuation increasing towards the tip of the rod.

The wavenumber estimates are clearly affected by the resonances of the sandbox which are responsible for the peaks in the dispersion curves. This can well be observed at low frequencies, where the attenuation is low, and close to the tip of the rod where the reflected wave has still a non-negligible amplitude over a broader frequency range.

5.2. Rod embedded in an infinite soil (axisymmetric model)

To verify the above observations further, we created another model in which the effect of the infinite soil is emulated. The model was defined as axisymmetric since the attention is focused on longitudinal waves only. The properties and dimensions of the rod and the contact conditions are the same as in the preceding section. The sand is now defined as a spherical domain with a radius of 1.5 m (properties kept the same) and a low reflective boundary specified on the outside surface of the sphere. The model consisted of 15797 quadratic triangular elements. An illustrative result for the axisymmetric model is shown in Figure 9(b).

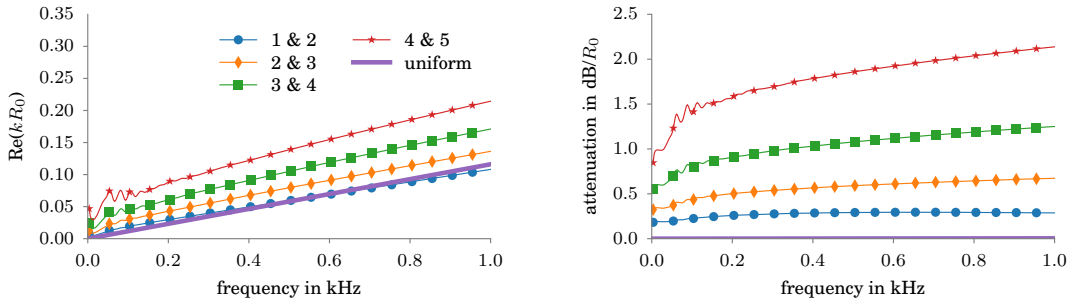

Figure 12. Wavenumbers for an exponential rod in an infinite sand domain calculated from different pairs of adjacent sensing locations.

Wavenumber estimates calculated from pairs of adjacent responses arranged in the same way as in the preceding section are presented in Figure 12. The performance of the low reflective boundary is very good except for the lowest frequencies (long wavelengths). The wave that travels along the rod radiates into the soil very effectively so that the amplitude at the tip is very small and hardly any reflection is observed (mainly in the estimate from sensors 4 and 5). The wavenumber is confirmed to be position dependent (increasing along the tapering), as well as the attenuation (increasing along the tapering as well). As expected, the sandbox resonances described earlier are no longer visible.

6. Conclusions

In this paper we considered longitudinal wave propagation in exponentially tapered circular rods. The focus was put on demonstrating the effects deduced from the well-established analytical solution experimentally. To achieve this, a measurement method, allowing for estimating wavenumbers from dynamic responses acquired at five equally spaced locations, was derived. The approach was tested in an experiment in which the wavenumbers in a wooden exponentially tapered rod were estimated. The results were shown to be in a very good agreement with the theoretical predictions. In the last part of the paper we investigated the effect of the surrounding medium on wave propagation in an embedded rod using finite element simulations. The cut-off phenomenon was no longer observed and the wavenumber was found to be position dependent,

as well as the attenuation. Waves radiated into the surrounding medium very effectively and little energy was carried don to the tip of the rod.

This paper is a preliminary part of the longer term investigation into remote tree root mapping. The fundamental physical characteristics discussed in this paper are rather well known. However, their association with tree roots has not been discussed to date. Moreover, our experimental approach is expected to facilitate future experiments on buried exponential bars emulating tree root networks. The observations presented in this paper indicate possible range limitations for vibroacoustic mapping methods.

Apart from the measurements on buried structures, we plan to develop an analytical/semi-analytical model for wave propagation in buried exponential bars with analytical absorbing boundary conditions. Depending on the coupling between the root and the soil, practical recommendations on the choice of excitation mechanism and processing of the results for effective and robust tree root detection will be proposed.

Acknowledgments
The authors gratefully acknowledge the financial support of the UK Engineering and Physical Sciences Research Council under grant EP/K021699/1. Finite element simulations were supported by the IRIDIS High Performance Computing Facility at the University of Southampton.

Appendix A. Forced response of an exponential rod

In this section the forced response calculation in the wave domain is detailed. A steady-state response is a superposition of waves travelling across a structure, hence it can be conveniently expressed using wave relationships [13]. The labelling for the waves at different stages is presented in Figure A1.

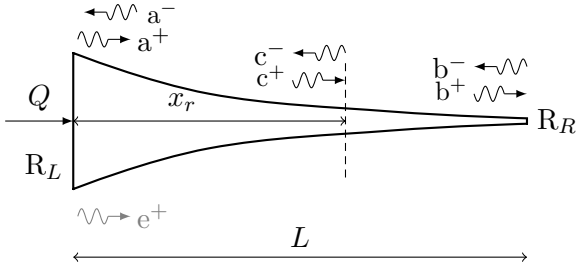

Figure A1. Schematic diagram of waves propagating along an exponentially tapered rod at different stages.

We consider a free-free rod excited by an axial force Q acting at the large face. The force induces a wave of amplitude e^+ which can be determined from force equilibrium at $x = 0$ (origin is where the force is applied)

$$P^+ + Q = 0 \tag{A.1}$$

with P^+ being the resultant force associated with longitudinal wave propagation. At $x = 0$

$$P^+(0) = EA(0)\frac{\partial u^+(x)}{\partial x}\bigg|_{x=0} = -\jmath k^+ EA(0)e^+ \tag{A.2}$$

Thus,

$$e^+ = \frac{-\jmath}{k^+ EA(0)} \tag{A.3}$$

The reflection coefficient at free ends is found from the equilibrium of forces associated with positive- and negative-going waves

$$R_R = -\frac{k^+}{k^-} \qquad \text{and} \qquad R_L = -\frac{k^-}{k^+} \tag{A.4}$$

The change of the wave amplitude along the waveguide axis is governed by propagation constants. As a consequence of tapering, they are different for positive- and negative-going waves

$$\tau^+(x) = \mathrm{e}^{-\jmath k^+ x} \qquad \text{and} \qquad \tau^-(x) = \mathrm{e}^{\jmath k^- x} \tag{A.5}$$

from where, e.g. $b^+ = \tau^+(L)a^+$ and $a^- = \tau^-(L)b^-$ (see Figure A1).

The travelling wave at the forcing location can be expressed as

$$a^+ = R_L a^- + e^+ \tag{A.6}$$

Accounting for the relationships between waves at different stages given by propagation and reflection matrices, we obtain the final expression for the steady-state wave amplitudes at the forcing location

$$a^+ = \left[1 - R_L \tau^- R_R \tau^+\right]^{-1} e^+ \tag{A.7}$$

and

$$a^- = \tau^- R_R \tau^+ a^+ \tag{A.8}$$

from which the point receptance can be written as

$$X_{\text{point}} = a^+ + a^- \tag{A.9}$$

whereas the transfer receptance at $x = x_r$ as

$$X_{\text{transfer}} = \tau^+(x_r)a^+ + \tau^-(L - x_r)R_R\tau^+(L)a^+ \tag{A.10}$$

References

[1] Morse P M 1936 *Vibration and Sound* (New York: McGraw-Hill)
[2] Stevenson A F 1951 *J. Appl. Phys.* **22** 1461–1463
[3] Nayfeh A H and Telionis D P 1973 *J. Acoust. Soc. Am.* **54** 1654–1661
[4] Junger M C and Cole III J E 1978 Dispersion and cut-off phenomena in rods and beams Tech. Rep. U-573-260 Cambridge Acoustical Associates
[5] Kumar B M and Sujith R I 1997 *J. Sound Vib.* **207** 721–729
[6] Langley R S 1999 *J. Sound Vib.* **227** 131–158
[7] Toso M 2004 *Wave propagation in rods, shells, and rotating shafts with non-uniform geometry* PhD Univ of Maryland
[8] Gan C, Wei Y and Yang S 2014 *J. Sound Vib.* **333** 434–445
[9] Wilson B F 1984 *The Growing Tree* (Amherst: Univ of Massachusetts Press)
[10] Muggleton J M, Brennan M J and Gao Y 2011 *J. Appl. Geophys.* **75** 54–61
[11] Graff K 1991 *Wave Motion in Elastic Solids* (New York: Dover)
[12] Muggleton J M, Brennan M J and Linford P W 2004 *J. Sound Vib.* **270** 171–190
[13] Mace B R 1984 *J. Sound Vib.* **97** 237–246